APPENDIX F

Computational Evaluation of the Steady and Pulsed Jet Effects on the Performance of a Circulation Control Wing Section

APPENDIX F

Computational Evaluation of the Steady and Pulsed Jet Effects on the Performance of a Circulation Control Wing Section

Yi Liu, Lakshmi N. Sankar, Robert Englar, K. Ahuja, R. Gaeta
Georgia Institute of Technology, Atlanta, GA 30332-1150

Introduction

Circulation Control Wing (CCW) technology is a very effective way of achieving very high lift coefficients needed by aircraft during take-off and landing. This technology can also be used to directly control the flow field over the wing. Compared to a conventional high-lift system, a Circulation Control Wing (CCW) can generate the required values of lift coefficient $C_{L,max}$ during take-off/ landing with fewer or no moving parts and much less complexity.

Earlier designs of CCW configurations used airfoils with a large radius rounded trailing edge to maximize the lift benefit. However, these designs also produced very high drag [1]. These high drag levels associated with the blunt, large radius trailing edge can be prohibitive under cruise conditions when Circulation Control is no longer necessary. To overcome this difficulty, an advanced CCW section, i.e., a circulation hinged flap [2, 3], was developed to replace the original rounded trailing edge CC airfoil. This concept developed by Englar is shown in Figure 1. The upper surface of the CCW flap is a large-radius arc surface, but the lower surface of the flap is flat. The flap could be deflected from 0 degrees to 90 degrees. When an aircraft takes-off or lands, the flap is deflected as in a conventional high lift system. Then this large radius on the upper surface produces a large jet turning angle, leading to high lift. When the aircraft is in cruise, the flap is retracted and a conventional sharp trailing edge shape results, greatly reducing the drag. This kind of flap does have some moving elements that increase the weight and complexity over an earlier CCW design. But overall, the hinged flap design still maintains most of the Circulation Control high lift advantages, while greatly reducing the drag in cruising condition associated with the rounded trailing edge CCW design.

In the present work, an unsteady three-dimensional Navier-Stokes analysis procedure has been developed and applied to this advanced CCW configuration. The solver can be used in both a 2-D and a 3-D mode, and can thus model airfoils as well as finite wings. The jet slot location, slot height, and the flap angle can all be varied easily and individually in the grid generator and the flow solver. Steady jets, pulsed jets, the leading edge and trailing edge blowing can all be studied with this solver.

APPENDIX F

Objectives of the Present Research

The objectives of the present research effort are to:

a) Develop a numerical analysis method to simulate the aerodynamics of advanced Circulation Control wing sections

b) Investigate the effects of blowing coefficient, angle of attack, free-stream velocity and jet slot height on the performance of the CC airfoil with steady jets

c) Evaluate the effects of pulsed jets on the performance of the CC airfoil, and assess the effects of the frequency of the pulsed jets on its performance

Mathematical and Numerical Formulation

Governing Equations

The Reynolds-averaged Navier-Stokes equations were solved in the present simulation. An unsteady three-dimensional compressible Navier-Stokes solver is being used. The solver can model the flowfield over isolated wing-alone configurations. Some applications of this solver on finite wings have been done by Kwon et al [4] and Bangalore et al [5]. Modifications of this solver have been made to model circulation control jets. Both 3-D finite wings and 2-D airfoils may be simulated with the same solver. Two turbulence models have been used: the Baldwin-Lomax [6] algebraic model and Spalart and Allmaras [7] one equation model.

Computational Grid

The construction of a high-quality grid about the CCW airfoil is made difficult by the presence of the vertical jet slot. In this solver, the jet slot is treated as a grid boundary as done by Shrewsbury[8, 9] and Williams and Franke[10]. A hyperbolic three-dimensional C-H grid generator is used in all the calculations. The three-dimensional grid is constructed from a series of two-dimensional C-grids with an H-type topology in the spanwise direction. The grid is clustered in the vicinity of the jet slot and the trailing edge to accurately capture the jet behavior over the airfoil surface.

The grid generation and the surface boundary condition routines are general enough so that one can easily vary the slot location, slot size, blowing velocity and direction of blowing.

APPENDIX F

Boundary Conditions

In CCW studies, the driving parameter is the blowing momentum coefficient, C_μ, defined as follows.

$$C_\mu = \frac{\dot{m}V_{jet}}{\frac{1}{2}\rho_\infty V_\infty^2 S} \tag{1}$$

Here, the jet mass flow rate is given by:

$$\dot{m} = \rho_{jet} V_{jet} A_{jet} \tag{2}$$

Conventional airfoil boundary conditions are applied everywhere except at the jet slot exit. Non-reflection boundary conditions are applied at the outer boundaries of C grid, and on the airfoil surface, adiabatic and no-slip boundary conditions are applied.

At the jet slot exit, the jet is set to be subsonic, and the following boundary conditions are specified at the slot exit: the total temperature of the jet, the momentum coefficient C_μ as a function of time, and the flow angle at the exit. In this simulation, the jet was tangential to the airfoil surface at the exit. All other parameters were computed using ideal gas law, and through an extrapolation of the latest solution static pressure distribution to the slot exit.

Results and Discussions

The advanced CCW airfoil studied with the body fitted grid is shown in Figure 2. The CCW flap setting may be varied both in the experiments and the simulations. The studies presented here are all for the 30 degree flap setting. In these studies, the free stream velocity was approximately 94.3 ft/sec at a dynamic pressure of 10 psf and an ambient pressure of 14.2 psia. The free stream density is about 0.00225 slugs/ft^3. These conditions have been chosen to closely match the experiments done by Englar et al [2]. These conditions translate into a free-stream Mach number 0.0836 and a Reynolds Number of 395,000.

Steady Jet Results:

Figure 3 shows the variation of lift coefficient with respect to C_μ at a fixed angle of attack (α=0 degree) for the CC airfoil with a 30-degree flap. Excellent agreement with measured data from experiment by Englar [2] is evident. It is seen that very high lift can be achieved by Circulation Control technology with a relatively low C_μ. A lift coefficient as high as 4.0 can be obtained at a C_μ value of 0.33, and the lift augmentation $\Delta C_l/\Delta C_\mu$ is greater than 10 for this 30-degree flap configuration.

APPENDIX F

Figure 4 shows the computed C_l variation with the angle of attack, for a number of C_μ values, along with measured data. It is found that the lift coefficient increases linearly with angle of attack until stall, just as it does for conventional sharp trailing edge airfoils. However, the increase of lift with angle of attack breaks down at high enough angles. This is due to static stall, and is much like that experienced with a conventional airfoil, but occurs at very high $C_{l,max}$ values, thanks to the beneficial effects of Circulation Control. The calculations also correctly reproduce the decrease in the stall angle observed in the experiments at high momentum coefficients. Unlike conventional airfoils, this is a leading edge stall. Figure 5 shows the streamlines around the CC airfoil at an angle of attack of 6 degrees, and C_μ = 0.1657. In this case, a leading edge separation bubble forms, that spreads over the entire upper surface resulting in a loss of lift. However, the flow is still attached at the trailing edge because of the strong Coanda effect.

Based on the above baseline results, a simulation was also to study the effects of the free-stream velocities on the lift and drag coefficients of the CC airfoil. In this case, the jet momentum coefficient, C_μ, is fixed at 0.1657, and the jet slot height is also fixed at 0.015 inch. However, the free-stream velocities are varying from 0.5 to 1.8 times of the experimental free-stream velocity, which is equal to 94.3 ft/sec, thus the jet velocity will vary with the free-stream velocity to keep a constant C_μ. As shown in Figures 6 and 7, for a given momentum coefficient, the lift coefficient and drag coefficient do not vary significantly with the change of the free-stream velocity except at the very low free-stream velocities. The reason for the production of low lift and high drag at low free-stream velocities is that the jet velocity is too low to generate a sufficiently strong Coanda effects that eliminates separation and the vortex shedding. It can be concluded that the performance of CC airfoils is independent of the free-stream velocity and the Reynolds number under the fixed C_μ and fixed jet slot height conditions, and that C_μ is an appropriate driving parameter for CC blowing if the slot-height is fixed.

Pulsed Jet Results:

The present computational studies were aimed at answering the following questions: Can pulsed jets be used to achieve desired increases in the lift coefficient at lower mass flow rates relative to a steady jet? What are the effects of the pulsed jet frequency on the lift enhancement at a given time-averaged C_μ? What is the optimum wave shape for the pulsed jet, i.e. how should it vary with time?

In the calculations below, the angle of attack was set at zero, and the dual-radius CC airfoil flap angle was fixed at 30 degrees. The shape of the CC airfoil, free-stream Mach number, slot height, chordwise location of the slot, and Reynolds number were all, likewise, held fixed as in the steady jet studies. In the present studies, the following variation of the momentum coefficient with time was assumed:

$$C_{\mu}(t) = C_{\mu,0}[1 + F(t)] \tag{3}$$

where, $C_{\mu,0}$ is the time-averaged momentum coefficient, which is also the value of the steady jet used for comparison. *F(t)* is a function of time, which varies from –1 to 1, and determines the temporal variation of the pulsed jet.

The sinusoidal pulsed jet is found not very effective compared to a square wave form pulsed jet due to higher mass flow rates required with sinusoidal jets. For square wave pulsed jets, Figures 8 and 9 show the variation of the time-averaged incremental lift coefficient ΔC_l over and above the base-line unblown configuration at three frequencies, 40 Hz, 120 Hz and 400 Hz. Figure 8 shows the variation with the average momentum coefficient $C_{\tilde{\mu}}$, and Figure 9 shows the variation with the average mass flow rate. For a given value of $C_{\mu,0}$, a steady jet gives a higher value of ΔC_l compared to a pulsed jet as shown in Figure 8. This is to be expected because the pulsed jet is operational only half the time during each cycle as where the steady jet is continuously on. The benefits of the pulsed jet are more evident in Figure 9. At a given mass flow rate, it is seen that the time-averaged values of lift are higher for the pulsed jet compared to the steady jet, especially at higher frequencies. Figures 10 show the variation of the average lift coefficient with the frequency. It is seen that higher frequencies are, in general, preferred over lower frequencies. For example, as shown in Figure 10, when the frequency is equal to 400 Hz, the square form pulsed jet only requires 73% of the average steady jet mass flow rate while it can achieve 95% of the lift achieved with a steady blowing.

For aerodynamic and acoustic studies, the frequency is usually expressed as non-dimensional quantity called the Strouhal number. A simulation has been done to calculate the average lift generated by the pulsed jet at fixed Strouhal numbers, which is defined as follows:

$$\mathrm{Str} = \frac{f\, L_{ref}}{U_{\infty}} \tag{4}$$

In the present study, for the baseline case, the L_{ref} is 8 inches, and the U_{∞} is equal to 94.3 ft/sec. For a 200 Hz pulsed jet, the Strouhal number is equal to 1.41.

From above equation, besides the frequency, there are other two parameters that could affect the Strouhal number, which are the free-stream velocity and L_{ref} (Chord of the CC airfoil). Thus, three cases have been studied. In the first case, as shown in Table 1, the free-stream velocity and the Chord of the CC airfoil are fixed, and the Strouhal number is varied with the change of frequency. In the second case, as shown in Table 2, the Strouhal number is fixed at 1.41 and the chord of the CC airfoil is also fixed. The frequency is varied along with the free-stream velocity to achieve the same Strouhal number. In the third case, as shown in Table 3, the Strouhal number is fixed at 1.41 and the free-stream velocity is also fixed, while the frequency is varied along with the chord of the CC airfoil. The Mach number and Reynolds number are also functions of the free-stream velocity and the airfoil chord, and were changed appropriately.

APPENDIX F

The time-averaged momentum coefficient, $C_{\mu,0}$, is fixed at 0.04 in these studies. Figure 11 shows the lift coefficient variation with the frequency for these three cases.

From tables 2 and 3, it is seen that the computed time-averaged lift coefficient varies less than 2% when the Strouhal number is fixed. Table 2 indicates that the same C_l can be obtained at a much lower frequency with a smaller free-stream velocity as long as the Strouhal number is fixed. Table 3 shows that for a larger configuration, the same C_l can be obtained at a lower frequency provided the Strouhal number is fixed. Table 1, on the other hand, shows that varying the frequency and Strouhal number while holding the other variables fixed can lead to a 12% variation in C_l. Thus, it can be concluded the Strouhal number has a more dominant effect on the average lift coefficient of the pulsed jet than just the frequency.

Additional Results and Discussions to be included in the full paper

In the full paper, the effects of the jet slot height on the performance of steady jets will be added. More detailed explanation and discussion about some results will also be included, especially an explanation for the improved performance for high frequency pulsed jets over steady jets.

References

1. Englar, R. J. and Huson, G. G., "Development of Advanced Circulation Control Wing High Lift Airfoils," AIAA paper 83-1847, presented at AIAA Applied Aerodynamics Conference, July, 1983.
2. Englar, Robert J., Smith, Marilyn J., Kelley, Sean M. and Rover, Richard C. III., "Application of Circulation Control to Advanced Subsonic Transport Aircraft, Part I: Airfoil Development," Journal of Aircraft, Vol.31 No.5, pp. 1160-1168, Sep. 1994.
3. Englar, Robert J., Smith, Marilyn J., Kelley, Sean M. and Rover, Richard C. III., "Application of Circulation Control to Advanced Subsonic Transport Aircraft, Part II: Transport Application," Journal of Aircraft, Vol.31, No.5, pp. 1169-1177, Sep. 1994.
4. Kwon, J. and Sankar, L.N., "Numerical Study of the Effects of Icing on Finite Wing Aerodynamics," AIAA Paper 90-0757.
5. Bangalore, A., Phaengsook, N. and Sankar, L. N., "Application of a Third Order Upwind Scheme to Viscous Flow over Clean and Iced Wings," AIAA Paper 94-0485.
6. Baldwin, B. S., and Lomax, H., "Thin Layer Approximation and Algebraic Model for Separated Turbulent Flows," AIAA Paper 78-257, Jan. 1978.

APPENDIX F

7. Spalart, P. R., and Allmaras, S. R., "A One-Equation Turbulence Model for Aerodynamic Flows," AIAA Paper 92-0439, Jan. 1992.
8. Shrewsbury, G. D., "Numerical Evaluation of Circulation Control Airfoil Performance Using Navier-Stokes Methods," AIAA paper 86-0286, January 1986.
9. Shrewsbury, G. D., "Numerical Study of a Research Circulation Control Airfoil Using Navier-Stokes Methods," Journal of Aircraft, Vol. 26, No. 1, pp.29-34, 1989.
10. Williams, S. L. and Franke, M. E., "Navier-Stokes Methods to Predict Circulation Control Airfoil Performance," Journal of Aircraft, Vol. 29, No.2, pp.243-249, March-April 1992.

APPENDIX F

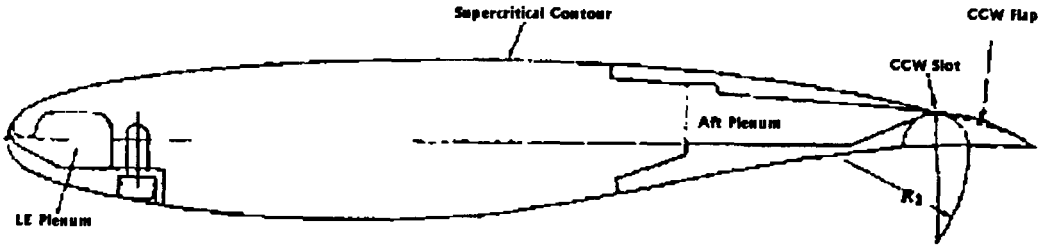

Figure 1. Dual Radius CCW Airfoil with LE Blowing [2]

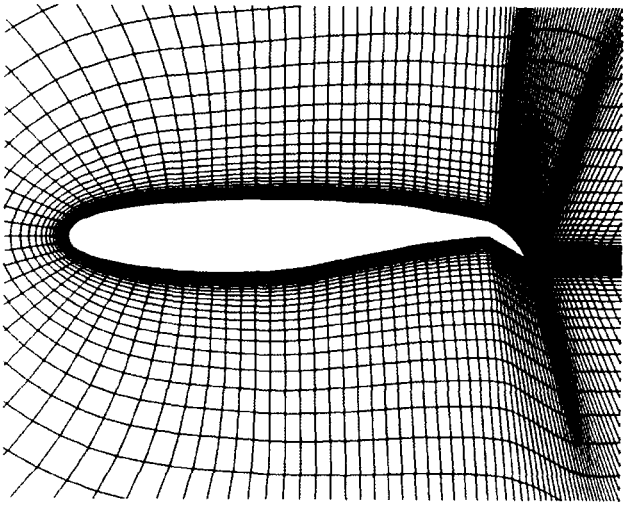

Figure 2. The Body-fitted C Grid near the CC Airfoil Surface.

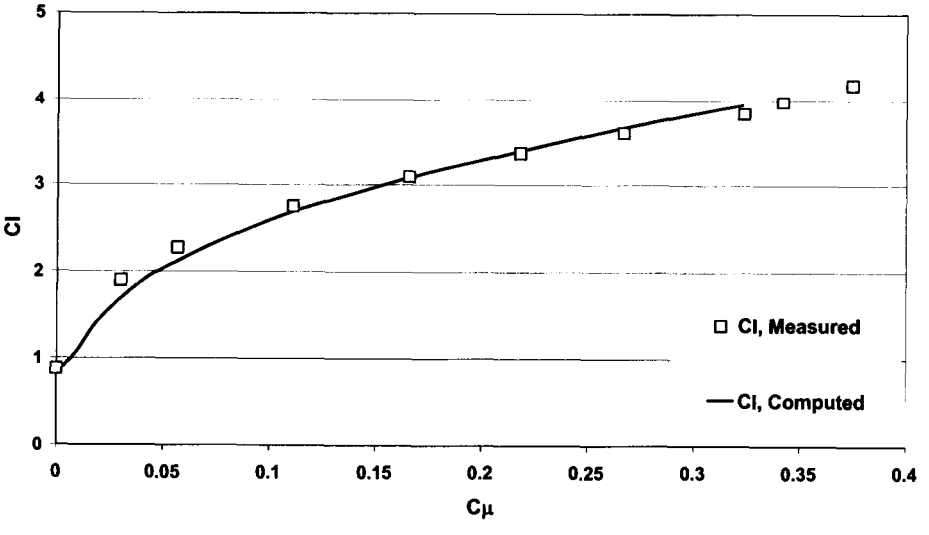

Figure 3. Variation of the Lift Coefficient with Momentum Coefficients at $\alpha=0°$

APPENDIX F

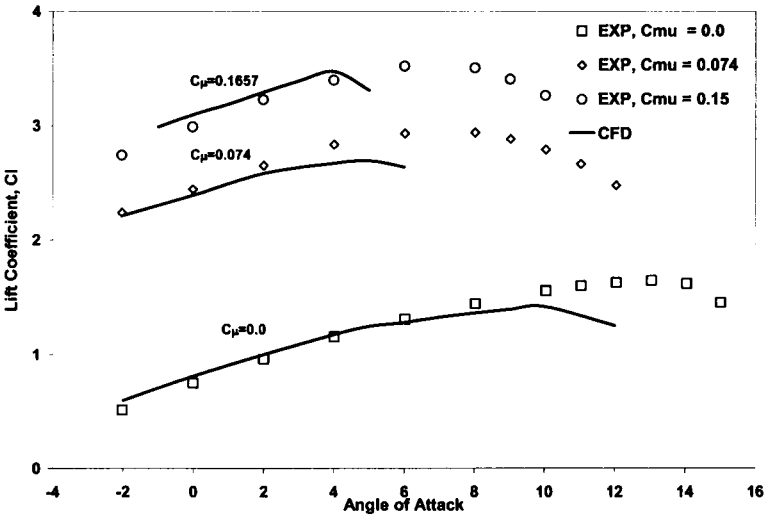

Figure 4. The Variation of the Lift Coefficient with Angle of Attack

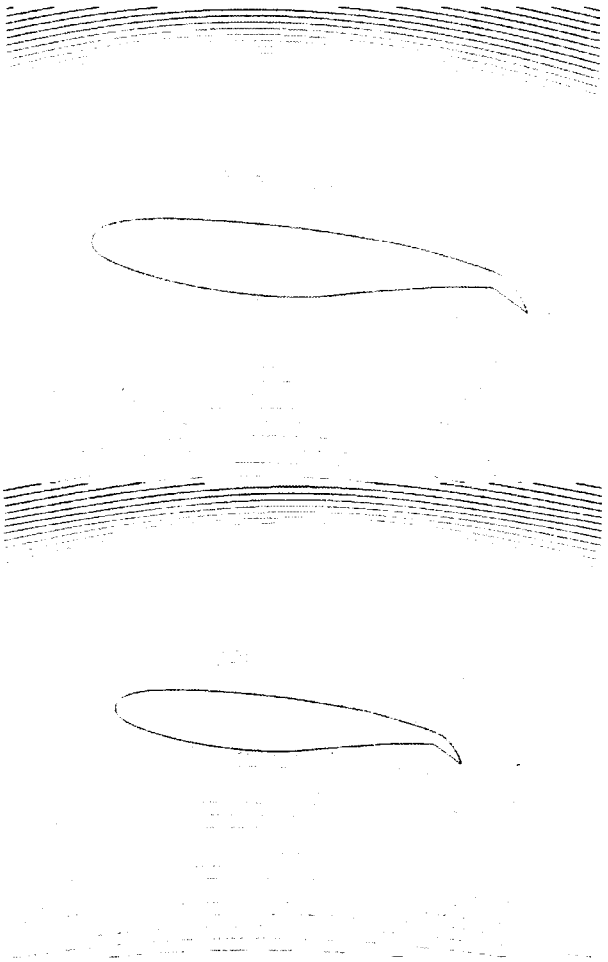

Figure 5. The Streamlines over the CC airfoil at Two Instantaneous Time Step ($C_\mu = 0.1657$, Angle of Attack = 6^0)

APPENDIX F

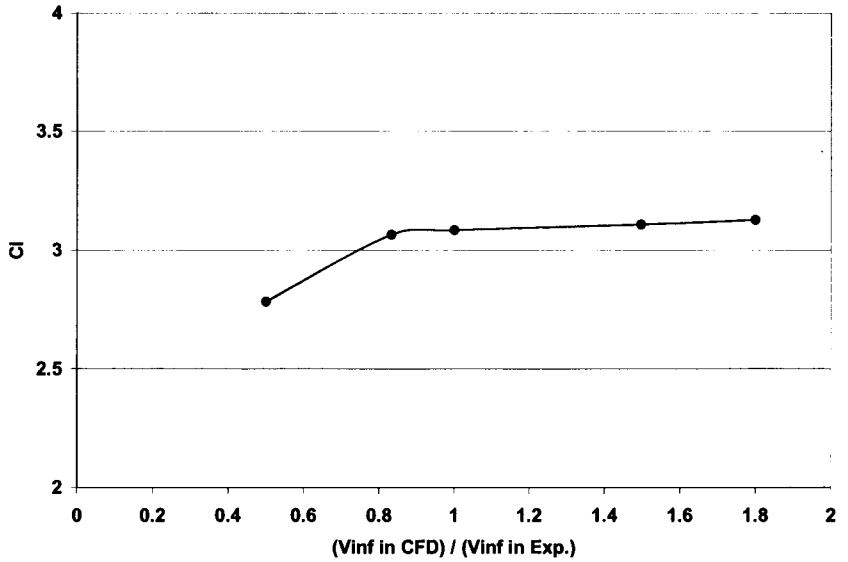

Figure 6. Lift Coefficient vs. Free-stream Velocity
(C_μ = 0.1657, h = 0.015 inch and $V_{\infty, exp}$ = 94.3 ft/sec)

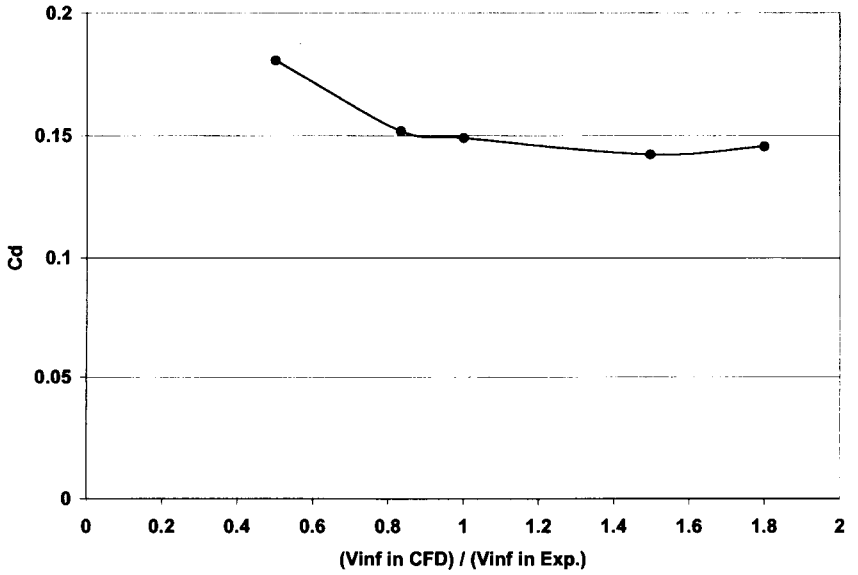

Figure 7. Drag Coefficient vs. Free-stream Velocity
(C_μ = 0.1657, h = 0.015 inch and $V_{\infty, exp}$ = 94.3 ft/sec)

APPENDIX F

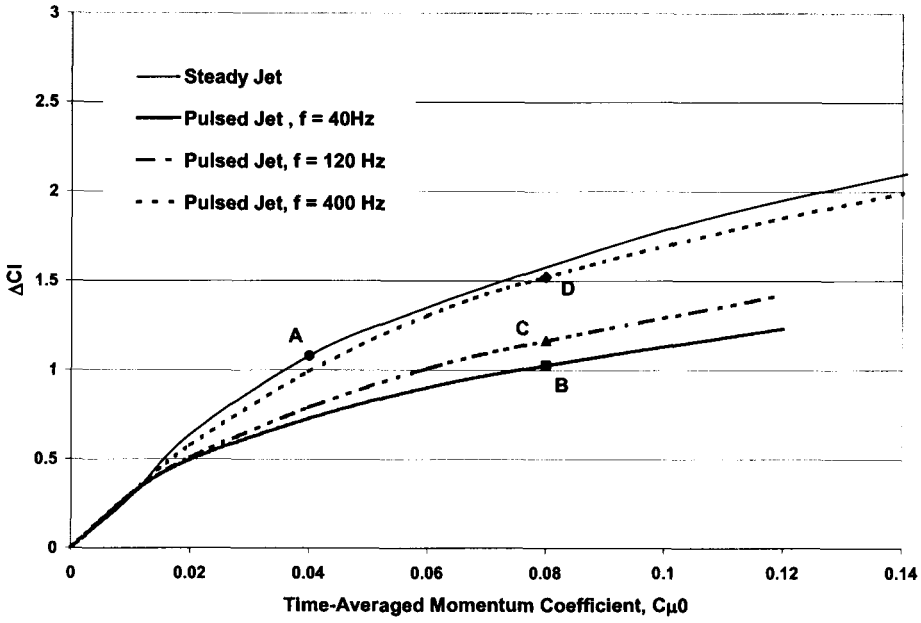

Figure 8. The Incremental Lift Coefficient vs. Time-averaged Momentum Coefficient

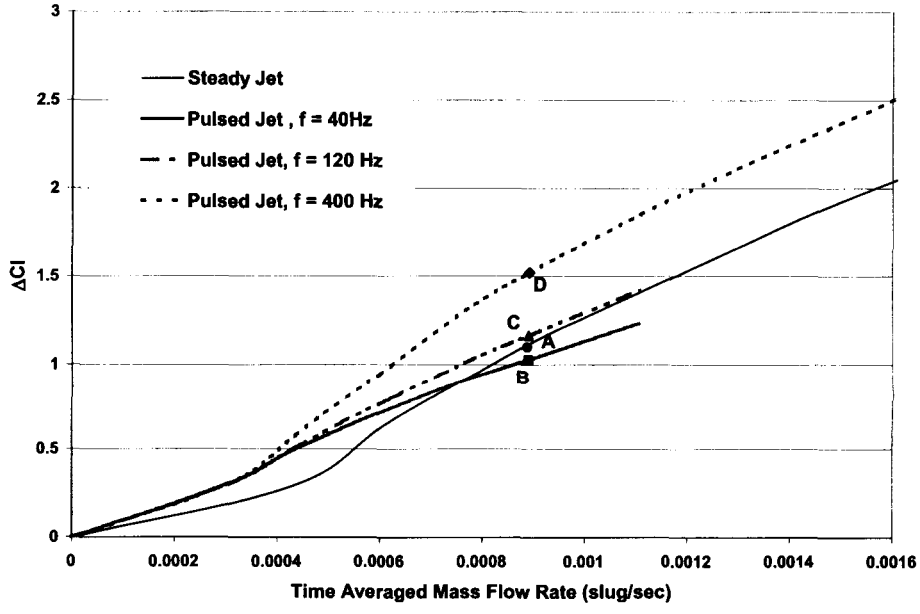

Figure 9. The Incremental Lift Coefficient vs. Time-averaged Mass Flow Rate

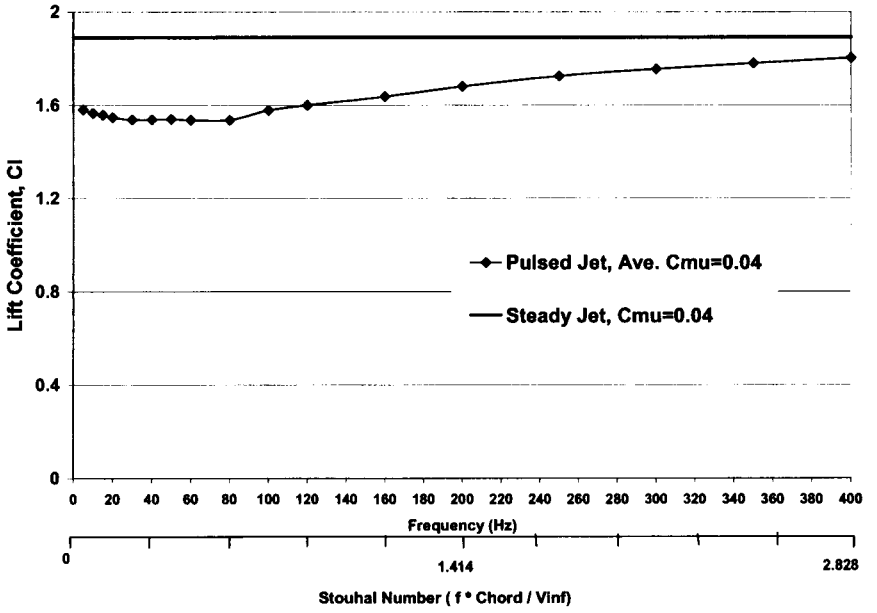

Figure 10. Time-averaged Lift Coefficient vs. Frequency & Strouhal Number

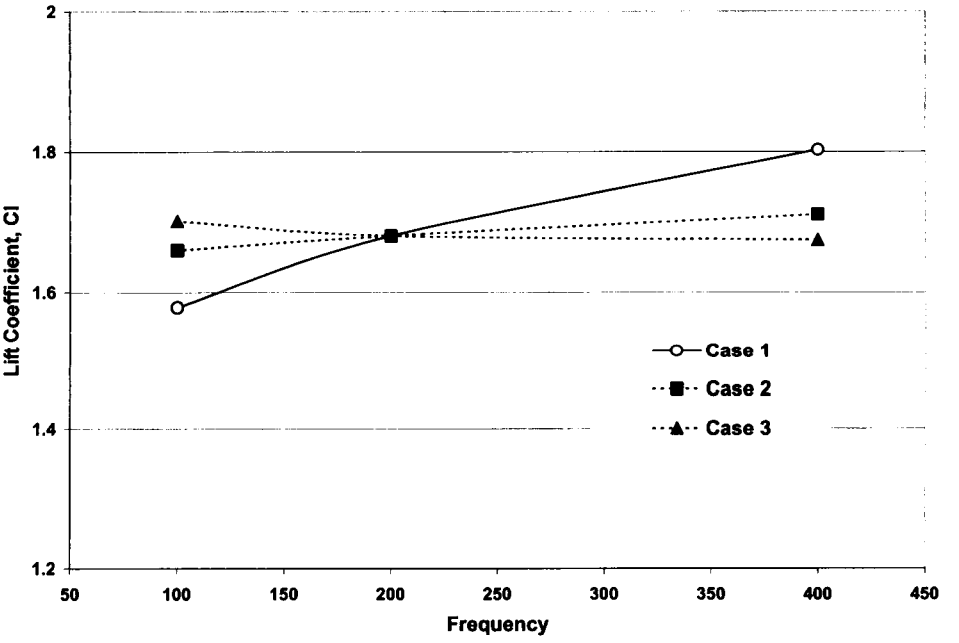

Figure 11. Time-averaged Lift Coefficient vs. Frequency

(Case 1. Strouhal number was not fixed; U_∞ and L_{ref} were fixed)
(Case 2. Strouhal number and L_{ref} were fixed; U_∞ was not fixed)
(Case 3. Strouhal number and U_∞ were fixed; L_{ref} was not fixed)

Table 1. The Computed Time-averaged Lift Coefficient for the Case one
(U_∞ and L_{ref} fixed, the Strouhal number varying with the frequency)

APPENDIX F

	Baseline	Half Frequency	Double Frequency
Frequency (Hz)	200	100	400
Free-Stream Velocity U_∞ (ft/sec)	94.3	94.3	94.3
Chord of the Airfoil L_{ref} (inch)	8	8	8
Strouhal Number	**1.41**	**0.705**	**2.82**
Computed Average Lift Coefficient (C_l)	**1.6804**	**1.5790**	**1.8026**

Table 2. The Computed Time-averaged Lift Coefficient for the Case Two
(Strouhal number and L_{ref} fixed, the U_∞ varying with the frequency)

	Baseline	Half Velocity	Double Velocity
Frequency (Hz)	200	100	400
Free-Stream Velocity U_∞ (ft/sec)	94.3	47.15	118.6
Chord of the Airfoil L_{ref} (inch)	8	8	8
Strouhal Number	**1.41**	**1.41**	**1.41**
Computed Average Lift Coefficient (C_l)	**1.6804**	**1.6601**	**1.7112**

Table 3. The Computed Time-averaged Lift Coefficient for the Case Three
(Strouhal number and U_∞ fixed, the L_{ref} varying with the frequency)

	Baseline	Double Chord	Half Chord
Frequency (Hz)	200	100	400
Free-Stream Velocity U_∞ (ft/sec)	94.3	94.3	94.3
Chord of the Airfoil L_{ref} (inch)	8	16	4
Strouhal Number	**1.41**	**1.41**	**1.41**
Computed Average Lift Coefficient (C_l)	**1.6804**	**1.7016**	**1.6743**